

# UCSF

## UC San Francisco Previously Published Works

### Title

Bioenergetic state regulates innate inflammatory responses through the transcriptional co-repressor CtBP

### Permalink

<https://escholarship.org/uc/item/1sz7m11h>

### Journal

Nature Communications, 8(1)

### ISSN

2041-1723

### Authors

Shen, Yiguo  
Kapfhamer, David  
Minnella, Angela M  
[et al.](#)

### Publication Date

2017

### DOI

10.1038/s41467-017-00707-0

Peer reviewed

**Bioenergetic state regulates innate inflammatory responses through the  
transcriptional co-repressor CtBP**

Yiguo Shen<sup>1,\*#</sup>, David Kapfhamer<sup>1,#</sup>, Angela M. Minnella<sup>1</sup>, Ji-Eun Kim<sup>1</sup>, Seok Joon Won<sup>1</sup>, Yanting  
Chen<sup>1,2</sup>, Yong Huang<sup>1</sup>, Ley Hian Low<sup>1</sup> Stephen M. Massa<sup>1</sup>, Raymond A. Swanson<sup>1\*§</sup>

<sup>1</sup> Department of Neurology, University of California, San Francisco, 94143, and San Francisco  
Veteran Affairs Medical Center, 4150 Clement St., San Francisco, CA 94121 USA

<sup>2</sup> Department of Neurology, Affiliated Drum Tower Hospital, Nanjing Medical University, Jiangsu,  
PR China

<sup>#</sup>These authors contributed equally to this work.

\*Current address: Adaptive Biotechnologies, 329 Oyster Point Blvd., South San Francisco, CA  
94080, USA

<sup>§</sup> Corresponding Author:

Raymond A. Swanson

(127) Neurology, SFVAMC

4150 Clement St., San Francisco, CA 94121 USA

[Raymond.Swanson@ucsf.edu](mailto:Raymond.Swanson@ucsf.edu)

Tel: (415) 750-2011; Fax: (415) 750-2273

30 **Abstract**

31 The innate inflammatory response contributes to secondary injury in brain trauma and other  
32 disorders. Metabolic factors such as caloric restriction, ketogenic diet, and hyperglycemia  
33 influence the inflammatory response, but how this occurs is poorly understood. Here we show  
34 that glucose metabolism regulates pro-inflammatory NF- $\kappa$ B transcriptional activity through effects  
35 on the cytosolic NADH:NAD<sup>+</sup> ratio and the NAD(H) sensitive transcriptional co-repressor, CtBP.  
36 Reduced glucose availability reduces the NADH:NAD<sup>+</sup> ratio, NF- $\kappa$ B transcriptional activity, and pro-  
37 inflammatory gene expression in macrophages and microglia. These effects are inhibited by forced  
38 elevation of NADH, reduced expression of CtBP, or transfection with an NAD(H) insensitive CtBP,  
39 and they are replicated by a synthetic peptide that inhibits CtBP dimerization. Changes in the  
40 NADH:NAD<sup>+</sup> ratio regulate CtBP binding to the acetyltransferase p300, and regulate binding of  
41 p300 and the transcription factor NF- $\kappa$ B to pro-inflammatory gene promoters. These findings  
42 identify a mechanism by which alterations in cellular glucose metabolism can influence cellular  
43 inflammatory responses.

44

45

46 **Keywords**

47 Glucose; metabolism; inflammation; p300; NF- $\kappa$ B; nicotinamide adenine dinucleotide; sirtuin

48

49

50

51

52 Microglia and macrophages exhibit a non-specific innate immune response to infection,  
53 tissue damage, and other stressors. The early phase of this response involves release of pro-  
54 inflammatory cytokines, nitric oxide, and metalloproteinases, along with alterations in cell  
55 morphology and surface protein expression<sup>1,2</sup>. While these responses are adaptive in the setting  
56 of infection, they can be deleterious in non-infectious injuries such as stroke and head trauma.  
57 Accordingly, factors that suppress the acute inflammatory reaction also reduce tissue loss and  
58 improve functional outcomes in animal models of non-infectious brain injury<sup>3,4</sup>.

59 Inflammatory responses are influenced at the transcriptional level by factors that affect  
60 cellular bioenergetic state, such as caloric restriction, ketogenic diet, and the glycolytic inhibitor 2-  
61 deoxyglucose (2DG)<sup>5,6</sup>. Caloric restriction, ketogenic diet, and 2DG each produce a ketogenic  
62 state in which glucose utilization is suppressed, and these conditions also reduce brain  
63 inflammation, tissue loss, and functional impairment after brain injury<sup>7,8,9,10,11,12</sup>. Conversely,  
64 hypoxia and hyperglycemia promote glucose utilization, exacerbate inflammation, and worsen  
65 outcomes after brain injury<sup>13,14</sup>.

66 How inflammation affects cell metabolism is well established<sup>15</sup>, but less is known about how  
67 energy metabolism affects inflammatory responses. One potential mechanism is through the  
68 cytosolic NADH:NAD<sup>+</sup> ratio, which is thermodynamically coupled to glycolysis. The cytosolic  
69 NADH:NAD<sup>+</sup> ratio is decreased by ketogenic factors such as dietary restriction and 2DG, which  
70 decrease flux through glycolysis, and increased by conditions such as hypoxia and hyperglycemia,  
71 which increase flux through glycolysis. Cytosolic NADH and NAD<sup>+</sup> are physically separated from the  
72 mitochondrial metabolite pools, but can move freely across the nuclear membrane to influence  
73 transcriptional events.

74 Despite the fundamental roles of NAD<sup>+</sup> and NADH in cell metabolism, only a limited number  
75 of NADH - sensitive proteins are known to affect gene transcription<sup>16</sup>. Among these are the C-  
76 terminal binding proteins (CtBPs), which function as transcriptional co-repressors. Mammals  
77 express two CtBP proteins, CtBP1 and CtBP2, that exhibit overlapping actions<sup>17,18</sup>. CtBP forms  
78 repressor complexes with histone deacetylases, histone methyl transferases, E3 ligases, and other  
79 transcriptional regulators<sup>19,20</sup>. Some of these complexes include CtBP homodimers or  
80 heterodimers, while others require CtBP in its monomeric form<sup>21,22,23,24</sup>. CtBP in its monomeric  
81 form suppresses the activity of the acetyltransferase p300/CBP<sup>20</sup>, which acetylates both histones

82 and the pro-inflammatory transcription factor, NF- $\kappa$ B<sup>25</sup>. Increased NADH levels promote the  
83 formation of CtBP dimers and higher order oligomers, and thereby modulate CtBP association with  
84 its binding partners<sup>26</sup>.

85 Here we investigate whether anti-inflammatory effects of ketogenic metabolism may be  
86 mediated through an NADH / CtBP signaling mechanism. We show that changes in cytosolic  
87 NADH:NAD<sup>+</sup> ratio influence inflammatory responses by regulating NF- $\kappa$ B transcriptional activity  
88 through a mechanism requiring CtBP dimerization. This process involves dissociation of p300 from  
89 CtBP and acetylation of the NF- $\kappa$ B p65 subunit.

90

## 91 **Results**

### 92 *Microglial and macrophage activation is suppressed by 2DG*

93 The reduced glycolytic flux resulting from caloric restriction and ketogenic diet can be mimicked  
94 by the glycolytic inhibitor 2-deoxyglucose (2DG)<sup>27,28</sup>. To determine if 2DG can replicate the effect  
95 of ketogenic diet on brain inflammatory responses, we treated rats with intraperitoneal injections  
96 of lipopolysaccharide (LPS) or with LPS + 2DG. The systemic LPS injection induced a robust  
97 activation of brain microglia, and this was strikingly reduced by co-administration of 2DG (Fig. 1A).  
98 In organotypic brain slice cultures (Fig. 1B), 2DG likewise suppressed the effect of LPS on microglial  
99 activation and on the expression of inducible nitric oxide synthase (iNOS), a hallmark of  
100 inflammatory activation in microglia and macrophages<sup>29</sup>. Primary microglial cultures similarly  
101 showed an attenuated response to LPS in the presence of 2DG (Fig. 1C), thus confirming that the  
102 effects of LPS and 2DG on microglia are not dependent upon indirect, systemic effects of these  
103 agents. This same pattern of responses was observed in the RAW264.7 macrophage cell line.  
104 RAW264.7 cells treated with LPS showed increased iNOS mRNA expression, iNOS protein  
105 expression, and nitric oxide production, all of which were attenuated by co-incubation with 2DG  
106 (Fig. 1D,E). RAW264.7 cells were used because, unlike primary microglia, they can be efficiently  
107 transfected and are not readily activated by transfection procedures. Glutamine was provided as  
108 an alternative energy substrate in all of the *in vitro* studies, as glutamine is taken up by cells and  
109 metabolized to the keto acid,  $\alpha$ -ketoglutarate. ATP measurements confirmed no significant effect  
110 of 2DG or glucose-free medium on ATP levels in the glutamine-supplemented cell cultures (Fig.  
111 1F).

112 *Glycolytic inhibition reduces cytosolic NADH:NAD<sup>+</sup> ratio*

113 We assessed the free cytosolic NADH:NAD<sup>+</sup> ratio by measuring the cellular lactate:pyruvate  
114 ratio<sup>30</sup>. This indirect approach has advantages over direct biochemical measurements in that it is  
115 not influenced by protein-bound or mitochondrial NAD<sup>+</sup> and NADH<sup>30,31</sup>. 2DG and glucose-free  
116 medium are predicted to lower the cytosolic (i.e. non-mitochondrial) NADH:NAD<sup>+</sup> ratio by  
117 decreasing glucose flux through glycolysis, while impaired respiration should increase glycolytic  
118 flux and elevate the cytosolic NADH:NAD<sup>+</sup> ratio (Fig. 2A). As expected, both 2DG and glucose -free  
119 medium reduced the lactate:pyruvate ratio (indicating a reduced free cytosolic NADH:NAD<sup>+</sup> ratio),  
120 while the respiratory inhibitors antimycin A and cobalt chloride (CoCl<sub>2</sub>)<sup>27,32</sup> increased it (Fig. 2B).  
121 We then evaluated these treatments on LPS-induced iNOS expression. Glucose-free medium  
122 suppressed LPS-induced iNOS expression to an extent comparable to that seen with 2DG, while  
123 CoCl<sub>2</sub> had the opposite effect (Fig. 2C). These findings identify a correlation between changes in  
124 the inflammatory response and changes in the NADH:NAD<sup>+</sup> ratio in response to metabolic factors.

125

126 *Elevated NADH reverses the anti-inflammatory effect of 2DG*

127 We next asked whether the metabolic influences on the inflammatory responses are blocked  
128 when changes in the NADH:NAD<sup>+</sup> ratio are negated. Lactate added to culture medium passes  
129 readily into cultured cells<sup>33</sup> and drives the NADH:NAD<sup>+</sup> equilibrium toward NADH (Fig. 2A), thus  
130 providing a means of countering the effect of glycolytic inhibition on the cytosolic NADH:NAD<sup>+</sup>  
131 ratio. The addition of sodium lactate (20 mM, pH 7.4) reversed the effects of glycolytic inhibition  
132 on LPS-induced iNOS expression in the cell cultures (Fig. 3A,B). Evaluation of iNOS gene  
133 transcription in cells transfected with an iNOS luciferase reporter gene confirmed an effect at the  
134 level of iNOS gene transcription (Fig. 3C).

135 The lactate:pyruvate ratio cannot be used in cells treated with lactate, so for these studies we  
136 instead evaluated changes in cytosolic NADH by measuring changes in intrinsic NAD(P)H  
137 fluorescence. This approach does not distinguish NADH from NADPH, but cellular NADPH levels are  
138 insensitive to acute changes in glycolysis or lactate<sup>34,35</sup>. Signal from mitochondrial NAD(P)H was  
139 avoided by sampling only from nuclei, which do not contain mitochondria (Fig. 3D). 2DG reduced  
140 the cytosolic NAD(P)H signal, in agreement with the lactate:pyruvate ratio determinations; and as  
141 expected 2DG had no effect on the mitochondrial NAD(P)H fluorescence (Fig. 3E). Glucose-free  
142 medium had comparable effects (Fig. 3F). The effects of both 2DG and glucose-free medium on

143 NAD(P)H levels were reversed by sodium lactate (20 mM, pH 7.4; Fig. 3F). Although lactate did not  
144 produce a significant increase in NAD(P)H signal when administered in the absence of 2DG (Fig.  
145 3F), the mitochondrial inhibitors cobalt and antimycin likewise failed to increase the NAD(P)H  
146 signal. NADH fluorescence measurements may be less sensitive to increases than to decreases in  
147 NADH because increased NADH is disproportionately protein-unbound, and NADH that is not  
148 protein bound has weaker intrinsic fluorescence<sup>36</sup>.

149

#### 150 *2DG suppresses NF-κB activated pro-inflammatory genes*

151 To evaluate the broader effects of 2DG on LPS-induced gene expression, we prepared  
152 microarrays from RAW264.7 cells after incubation under control, LPS, or LPS+2DG conditions.  
153 Expression levels of 994 genes were significantly affected by LPS and 781 by LPS+2DG, with 579  
154 genes responding to both conditions (Fig. 4A). An analysis of transcription factor binding sites on  
155 these genes showed that conserved NF-κB family binding sites (Rel and RelA/p65) were over-  
156 represented in the LPS+2DG condition (Supplemental Table 1; Supplemental Data Sets 1 and 2), as  
157 would be expected given the dominant role of NF-κB in pro-inflammatory transcriptional  
158 responses. RT-PCR quantifications of specific NF-κB - driven pro-inflammatory gene transcripts,  
159 *IL1B*, *IL6*, and *iNOS*, confirmed that they were upregulated by LPS, and that 2DG suppressed their  
160 upregulation (Figs. 1D, 4B).

161

#### 162 *The anti-inflammatory effect of 2DG is mediated by CtBP*

163 We next evaluated whether the NAD(H)-sensitive transcriptional co-repressor, CtBP, is  
164 involved in the process by which energy metabolism influences inflammation. We generated a  
165 stable CtBP knockdown RAW264.7 cell line using lentivirus that expressed shRNA targeting a  
166 sequence that, in mice, is present only in *CtBP1* and *CtBP2*. The CtBP knockdown cell line displayed  
167 a  $98.9 \pm 0.2$  % reduction in *CtBP1* and  $80.8 \pm 4$  % reduction in *CtBP2* transcripts, and a  $64 \pm 10$  %  
168 reduction in CtBP1/2 protein expression (Fig. 5A). Like wild-type cells, CtBP knock-down cells  
169 responded to LPS with increased iNOS expression and NO production (though to a lesser extent);  
170 however, unlike wild-type cells, CtBP knockdown cells showed no suppression of this response  
171 when treated with 2DG or glucose-free medium (Fig. 5B,C). Similarly, the effect of 2DG on LPS-  
172 induced NF-κB transcriptional activity was not observed in the CtBP knock-down cells (Fig. 5D), nor

173 was the effect of 2DG on LPS-induced *iNOS*, *Il1B*, and *Il6* gene expression (Fig. 5E; compare to Figs.  
174 1D, 4B).

175 If transcriptional effects of cytoplasmic NADH : NAD<sup>+</sup> ratio are mediated by CtBP, then they  
176 should be diminished in cells expressing an NAD(H) - insensitive CtBP. The G189A mutation in  
177 CtBP2 disrupts its binding to NAD(H) while preserving its co-repressor activity<sup>27</sup>. We therefore  
178 determined whether the G189A mutation would negate the effect of NADH elevations on NF-κB –  
179 mediated transcriptional responses. Studies were performed in CtBP1<sup>-/-</sup>/CtBP2<sup>-/-</sup> MEF cells in order  
180 to eliminate effects of endogenous CtBP1/2 (Fig. 6A), and because the shRNA expressed by the  
181 stable CtBP knockdown RAW264.7 cell line precludes expression of the mutant CtBP in those cells.  
182 The MEF cells were transfected with either wild-type (wt) CtBP1, wt CtBP2, or mutant G189A  
183 CtBP2 (Fig. 6A). Since the MEF cells responded only weakly to LPS (not shown) an NF-κB  
184 transcriptional response was induced by co-transfection with the p65 subunit of NF-κB. All three of  
185 the CtBP constructs suppressed NF-κB transcriptional activity, consistent with the potent co-  
186 repressor activity of CtBP (Fig. 6B-D). Treatment with 2DG produced no further reduction in this  
187 already suppressed NF-κB activity; however, treatment with CoCl<sub>2</sub>, which elevates the NADH :  
188 NAD<sup>+</sup> ratio, increased NF-κB activity in cells expressing wt CtBP2, but not in cells expressing G189A  
189 mutant CtBP2 (Fig. 6E). This pattern was also observed in primary microglia: CoCl<sub>2</sub> augmented LPS-  
190 induced *iNOS* expression in microglia overexpressing wild-type CtBP, but not in microglia  
191 overexpressing G189A CtBP2 (Fig. 6F).

192 Given that CtBP overexpression suppresses NF-κB transcriptional activity (Fig. 6C,D) we also  
193 evaluated the possibility that 2DG effects on LPS-induced responses might be caused by  
194 upregulated CtBP expression, independent of the CtBP responses to cytosolic NADH : NAD<sup>+</sup> ratio.  
195 However, measures of CtBP mRNA levels in primary microglia showed that 2DG did not increase  
196 expression of either CtBP1 or CtBP2, with or without LPS co-treatment (Suppl. Fig. 1A,B).

197

### 198 *Peptide inhibition of CtBP dimerization*

199 To further evaluate the mechanism by which CtBP regulates inflammatory responses, we  
200 generated a synthetic peptide that blocks CtBP dimerization. Examination of the crystal structure  
201 of a rat CtBP dimer complexed with NAD(H)<sup>37</sup> suggested that a peptide near the center of the  
202 dimerization region, if stably folded, could bind to the CtBP monomer and interfere with dimer  
203 formation. This dimerization region contains two alpha helical domains that are structurally

204 conserved in CtBP family members, and contains four residues that, when mutated, prevent  
205 dimerization of drosophila CtBP<sup>22</sup>. A peptide spanning this region, corresponding to amino acids 114-  
206 142 of the long form of mouse CtBP1 (Fig. 7A), and a control peptide lacking any known effects on  
207 cell function were generated and fused to N-terminal Tat sequences (CPC Scientific (Sunnyvale,  
208 CA). The CtBP peptide sequence was GRKKRRQRRRCVEETADSTLCHILNLYRRTTWLHQALREG (with  
209 the Tat sequence underlined), and the control peptide sequence was  
210 GRKKRRQRRRCCSFNSEYELGSLCYGRKKRRQRR. To determine if the CtBP peptide could block CtBP  
211 dimerization in vitro, we co-expressed CtBP1-HA and CtBP1-Flag tagged constructs in COS7 cells  
212 and performed immunoprecipitation with antibody to Flag. Very little HA-tagged CtBP was  
213 immunoprecipitated with anti-Flag antibody in untreated control samples (Fig. 7B), suggesting that  
214 the majority of the CtBP-tagged protein is monomeric. In contrast, in vitro treatment of lysate with  
215 100 mM lactate plus 10  $\mu$ M NADH for 20 minutes prior to immunoprecipitation (to force an  
216 increase in the NADH:NAD<sup>+</sup> ratio in the lysates) greatly increased the amount of CtBP1-HA  
217 associated with CtBP-Flag. This association was disrupted by co-incubation with 50  $\mu$ M of the CtBP  
218 peptide (Fig. 7B).

219 We next tested whether the CtBP peptide could inhibit LPS-induced inflammatory gene  
220 expression, as observed in the 2DG - induced ketogenic state. Primary microglia were treated with  
221 LPS, alone or in combination with 5  $\mu$ M CtBP peptide or control peptide. The CtBP peptide  
222 reduced LPS-induced iNOS, IL-1b and IL-6 transcript expression, while the control peptide had no  
223 effect (Fig. 7C). We then evaluated whether the CtBP peptide could block inflammatory gene  
224 expression in vivo. In initial experiments, we treated mice intraperitoneally with 2DG (100 mg / kg)  
225 10 minutes prior to stereotactic injection of 8  $\mu$ g LPS into the left striatum. Three hours post-  
226 surgery, brains were removed and microglia were isolated from the striatum for gene expression  
227 studies. These studies confirmed that LPS robustly induces iNOS expression in microglia in vivo,  
228 and that this effect is attenuated by 2DG (Fig. 7D). We then co-injected LPS (8  $\mu$ g) along with the  
229 CtBP peptide or control peptide into the striatum 3 hours prior to microglial isolation. The LPS-  
230 induced increase in iNOS gene expression was reduced by the CtBP peptide, but not by the control  
231 peptide. In contrast, LPS-induced expression of the M2-type anti-inflammatory gene, Socs3  
232 (Suppressor of cytokine signaling 3)<sup>38</sup>, was unaffected by CtBP peptide, demonstrating that the  
233 peptide does not exert a global or nonspecific effect on transcription (Fig. 7E,F).

234

235 *p300 binding to CtBP and pro-inflammatory gene promoters*

236 One way that CtBP regulates gene transcription is through interactions with the histone  
237 acetyltransferase HDAC1<sup>19</sup>. We therefore performed chromatin immunoprecipitation (ChIP)  
238 targeting the IL-6 promoter to evaluate the effects of ketogenic state on HDAC1 binding and  
239 histone H3 acetylation. Both HDAC1 binding and H3 acetylation were increased in cells treated  
240 with LPS, but neither was reversed by 2DG (Fig. 8A). A second way that CtBP regulates gene  
241 transcription is by repressing the activity of p300<sup>20,39</sup>, which acetylates and thereby promotes the  
242 activity of transcription factors such as the p65 subunit of NF- $\kappa$ B<sup>25</sup>. The ChIP studies showed that  
243 LPS induced p65 binding to the IL-6 promoter, and that this was completely reversed in the  
244 presence of 2DG (Fig 8A). This effect of 2G was accompanied by parallel changes in p65  
245 acetylation status, as assessed by western blots from cells treated with LPS or LPS + 2DG (Fig. 8B).  
246 Additional ChIP studies showed that LPS induced p300 binding to the IL-6, IL-1b, and iNOS  
247 promoter regions, and that 2DG markedly attenuated each of these effects (Fig. 8C). These results  
248 parallel the effects of LPS and 2DG on iNOS, IL1B, and IL6 mRNA and protein expression (Figs. 1, 4).  
249 We then performed co-immunoprecipitation of p300 with CtBP in cells transfected with either  
250 wild-type CtBP2 or G189A CtBP2 to confirm that p300 binding to CtBP is similarly sensitive to  
251 NADH. 2DG - induced reductions in the cytosolic NADH:NAD<sup>+</sup> ratio did not increase the binding of  
252 p300 to either wild-type CtBP2 or G189A CtBP2, presumably because binding was already  
253 saturated by CtBP overexpression; however, CoCl<sub>2</sub> - induced elevations in the NADH:NAD<sup>+</sup> ratio  
254 reduced the binding of p300 to wild-type CtBP, but not G189A CtBP2 (Fig. 8D,E).

255

## 256 **Discussion**

257 CtBP has previously been shown to mediate effects of cellular metabolic state on  
258 transcriptional events contributing to cancer and epilepsy<sup>27,40</sup>. The present findings demonstrate  
259 that CtBP similarly couples metabolic state to the innate inflammatory response. They show that  
260 the pro-inflammatory gene expression and NF- $\kappa$ B transcriptional activity induced by LPS are  
261 coupled to glucose metabolism by the cytosolic NADH:NAD<sup>+</sup> ratio, and that this coupling is  
262 attenuated by CtBP downregulation, by forced elevation of NADH, by transfection with an NADH -  
263 insensitive CtBP, and by a synthetic peptide that blocks NADH - induced CtBP dimerization. They  
264 additionally show that metabolic state influences CtBP binding to the acetyltransferase p300, p300

265 binding at pro-inflammatory gene promoter sites, and acetylation state of NF- $\kappa$ B. The  
266 observations suggest a mechanism by which the liberation of CtBP from its dimerized form by  
267 lowered cytosolic NADH levels can suppress pro-inflammatory gene transcription.

268 The initial observation by Zhang et al.<sup>26</sup> that NADH binding promotes CtBP dimerization  
269 suggested that CtBP could regulate transcription in response to metabolic changes. Subsequent  
270 studies confirmed that CtBP mediates effects of 2-deoxyglucose, hypoxia, pyruvate, and other  
271 metabolic influences on gene expression<sup>27,41</sup>. Since NAD<sup>+</sup> and NADH recognize the same binding  
272 site on CtBP, changes in the concentration of either nucleotide could, in principle, regulate CtBP  
273 interactions with its binding partners. However, the relative changes in NADH caused by shifts in  
274 the cytosolic NADH:NAD<sup>+</sup> ratio are several hundred-fold greater than the reciprocal changes in  
275 NAD<sup>+</sup> because the cytosolic NADH : NAD<sup>+</sup> ratio is normally in the range of 1:700<sup>35</sup>. The sensitivity  
276 of CtBP to changes in NADH thus makes it particularly responsive to changes in energy metabolism  
277<sup>42</sup>. Inflammatory responses can also be modulated by NAD<sup>+</sup> - dependent de-acetylases of the  
278 sirtuin family, notably Sirt1<sup>43</sup>, but unlike CtBP sirtuins are not responsive to changes in NADH  
279 concentrations, and it remains uncertain whether their activity is significantly affected by the  
280 relatively small changes in NAD<sup>+</sup> concentrations that result from changes in energy metabolism<sup>44</sup>.

281 CtBP1 and CtBP2 have nearly identical amino acid sequences and share the same NAD(H)  
282 binding site. CtBP1 lacks a putative nuclear localization signal, but may enter the nucleus as  
283 heterodimer with CtBP2 or other proteins<sup>22,45</sup> and may also interact in the extra-nuclear cytosol  
284 with binding partners such as p300 and HDAC1. CtBP2<sup>-/-</sup> mice are nonviable, but CtBP1<sup>-/-</sup> mice are  
285 viable and fertile. Mice with combinations of CtBP1 and CtBP2 mutant alleles exhibit gene dosage-  
286 sensitive defects in several developmental processes<sup>17</sup>. Specific defects in immune function were  
287 not reported in these mutants, but CtBP has elsewhere been shown to modulate the role of  
288 estrogen receptors on inflammatory responses mediated by the AP-1 transcription factor,  
289 independent of metabolic changes<sup>46</sup>.

290 CtBP regulates gene transcription in multiple ways, including interactions with histone  
291 deacetylases, histone methyl transferases, and E3 ligases, and the p300 acetyltransferase. We did  
292 not find changes in histone acetylation or HDAC1 binding at pro-inflammatory gene promoters in  
293 response to a ketogenic state, but did find decreased binding of p300 and decreased acetylation of  
294 p65, which is a substrate for p300<sup>25</sup>. Since p65 acetylation increases NF- $\kappa$ B transcriptional activity,  
295 these findings identify a mechanism by which metabolic effects on CtBP can modulate gene

296 transcription. However, both monomer and dimer forms of CtBP can affect gene transcription<sup>21, 22,</sup>  
297 <sup>23, 24</sup>, and our findings do not establish that p300/CtBP binding is essential for the observed effects  
298 of CtBP on pro-inflammatory gene transcription. CtBP2 could alternatively directly associate with  
299 p65 and suppress its acetylation by a mechanism independent of dimer/monomer transition or  
300 p300 inhibition<sup>47</sup>. Recent studies have also identified alternative ways that glucose metabolism  
301 can influence inflammatory responses, including effects on HDAC4 protein levels, NLRP3  
302 inflammasome formation, and the activation of RAGE receptors<sup>48, 49, 50</sup>.

303 Cell cultures were used in our studies to facilitate manipulation of CtBP expression and  
304 cellular cytosolic NADH:NAD<sup>+</sup> ratios. A limitation cell cultures, and cell lines in particular, is a shift  
305 from respiratory ATP production toward more glycolytic ATP production (the Warburg effect<sup>51</sup>).  
306 Moreover, the glucose concentration in standard culture media is saturating for glucose uptake  
307 and metabolism. As a consequence, basal glycolytic flux is typically much higher in culture  
308 preparations than in vivo. This may explain why relatively larger shifts in the cytosolic NADH : NAD<sup>+</sup>  
309 ratio were observed with glycolytic inhibition than with respiratory inhibitors. However, the anti-  
310 inflammatory effects of 2DG in the cell culture preparations were also observed in vivo, as initially  
311 reported several decades ago<sup>6</sup>. Importantly, these results were also mimicked, both in vitro and  
312 in vivo, by the use of a novel synthetic peptide that inhibits NADH-induced CtBP dimerization. This  
313 result agrees with the prior observation that native CtBP1 represses p300 activity in an NADH -  
314 dependent manner, whereas dimerization-incompetent CtBP1 represses p300 activity  
315 independent of NADH<sup>20</sup> It may be surprising that reduced CtBP expression did not itself lead to a  
316 super-induction of iNOS and related genes, given co-repressor actions of CtBP. However, a  
317 reduction in total CtBP does not necessarily produce a comparable reduction in nuclear  
318 monomeric CtBP.

319 Taken together, our findings indicate that metabolic influences that alter the cytosolic NADH :  
320 NAD<sup>+</sup> ratio regulate NF-κB transcriptional activity through an NADH-dependent effect on CtBP  
321 dimerization. Conditions that reduce glycolytic flux, such as ketogenic diet and caloric restriction,  
322 can thereby suppress NF-κB activity, while conditions that increase glycolytic flux may increase it.  
323 These interactions provide a mechanism for the suppressive effects of ketogenic diet and caloric  
324 restriction on brain inflammation after brain injury. By extension, these interactions may also  
325 contribute to the pro-inflammatory states associated with diabetes mellitus and metabolic  
326 syndrome<sup>15, 52, 53</sup>.

327

328 **Methods**

329 Reagents

330 The MEF cell lines (*CtBP1*<sup>-/-</sup>/*CtBP2*<sup>-/-</sup> and *CtBP1*<sup>-/+</sup>/*CtBP2*<sup>-/+</sup>) were a kind gift from Dr. A. Roopra  
331 (University of Wisconsin, Madison). HEK293 cells and the macrophage-derived RAW264.7 cell line  
332 were obtained from the ATCC. The p*NF-κB-RE*-firefly and pRL-CMV renilla luciferase reporter  
333 were obtained from Promega, and the control pTA-luciferase reporter was obtained from  
334 Panomics. Full-length cDNAs of mouse *CtBP1* and *CtBP2* were cloned into pIRES-hrGFP-1a  
335 (Agilent) from adult mouse brain cDNA by reverse transcriptase PCR. The CtBP2 G189A mutant  
336 was a gift from Dr. J. Blaydes (University of Southampton, UK) and was cloned into pIRES-hrGFP-  
337 1a. The *iNOS* promoter-luciferase reporter was a gift from Dr. C. Lowenstein (University of  
338 Rochester, Addgene plasmid 19296)<sup>54</sup>, the p300 plasmid was a gift from Dr. W. Sellers (Dana-  
339 Farber Cancer Institute, Addgene plasmid 10717), the p65 plasmid was a gift from Dr. W. Greene  
340 (UCSF, Addgene plasmid 21966), and the flag-tagged CtBP2 plasmid was a gift from Dr. A. Roopra  
341 (University of Wisconsin, Madison). GIPZ-puro vector-based lentiviral vectors containing CtBP1/2  
342 shRNA were purchased from Open Biosystem (Thermo Scientific), and purified lentivirus  
343 transduction particles were generated by the UCSF ViraCore Laboratory. All constructs were  
344 sequence verified. All other reagents were obtained from Sigma-Aldrich except where noted.

345

346 *Surgical procedures and microglial isolation:*

347 Studies were approved by the San Francisco Veterans Affairs Medical Center animal studies  
348 committee. Male Sprague-Dawley rats, age 4-6 months (Charles River Laboratories), were given  
349 intraperitoneal injections of LPS (10 mg/kg) or saline vehicle, with or without 2-deoxyglucose  
350 (2DG; 100 mg/kg)<sup>55</sup>. Twenty four-hours later the rats were anesthetized and perfused with saline  
351 followed by 4% formaldehyde. Coronal 40 μm cryostat sections were prepared and  
352 immunostained<sup>56</sup> for CD11b (Serotec, clone OX-42, 1:100 dilution). Images were acquired using  
353 fluorescence confocal microscope and quantified as described<sup>57</sup>.

354 Stereotaxic LPS injections were performed in adult male C57BL/6J mice that were anesthetized  
355 with 2% isoflurane. The left striatum (A 1.3, ML 1.9, DV 3.5 mm from Bregma and the cortical  
356 surface) was injected with 8 μg LPS and 5 pmole CtBP peptide or control peptide in a volume of 5  
357 μl sterile saline over 25 min (0.2 μl/min). Three hours later the mice were transcardially perfused

358 with saline to remove circulating macrophages. After perfusion, brains were quickly removed and  
359 the left anterior quadrant containing the infusion site (approximately 100 mg tissue) was dissected  
360 and placed in ice cold Hank's Balanced Salt Solution (HBSS) without  $\text{Ca}^{2+}$  and  $\text{Mg}^{2+}$ . Tissue was  
361 briefly minced with a sterile razor blade and cells were dissociated using Neural Tissue Dissociation  
362 Kit (P) and Octo Dissociator (Miltenyi Biotec, San Diego, CA). Microglia were isolated using CD11b  
363 MicroBeads (Miltenyi Biotec). Accuracy of cell separation was validated by expression profiling of  
364 cellular fractions using quantitative PCR primers specific to microglia (Iba1 forward: 5'-  
365 GAAGCGAATGCTGGAGAAAC, reverse: 5'-GACCAGTTGGCCTCTTGTGT), neurons (NeuN forward: 5'-  
366 GGAACAGTCTATGGGCCTGA, reverse: 5'-ACAAGAGAGTGGTGGGAACG ) and astrocytes (GFAP  
367 forward: 5'-AGAAAGGTTGAATCGCTGGG, reverse: 5'-CGGCGATAGTCGTTAGCTTC) (Supplementary  
368 Fig. 2).

369

#### 370 *Hippocampal organotypic slice cultures*

371 Slice cultures were prepared as described<sup>58</sup>, with minor modifications. Brains were removed  
372 from 4-day old male mice C57BL/6 mice, and 350  $\mu\text{M}$  sagittal sections were prepared with a  
373 vibratome in ice cold dissecting media. The hippocampi were placed on Millicell inserts in 6 well  
374 culture plates, and maintained for 2 weeks at 37°C in 5%  $\text{CO}_2$ / 95% air incubator. Experiments  
375 were initiated by adding 10  $\mu\text{g}$  / ml LPS  $\pm$  1 mM 2DG. After 24 hours the slices were fixed with 4%  
376 formaldehyde. Slices were immunostained using rabbit polyclonal antibody to Iba1 (Wako #019-  
377 19741; 1:200 dilution) and rabbit polyclonal antibody to iNOS (Millipore, # 06-573; 1:250 dilution).

378

#### 379 *Cell cultures*

380 Mouse primary microglia cells were isolated and cultured as described<sup>56</sup> and used after 10  
381 days in vitro. Cell lines were seeded at a density of  $1 \times 10^4$  cells / well in 24-well plates one day  
382 prior to the experiments. For protein expression and luciferase assays, MEF cells, RAW264.7 cells  
383 and HEK293 cells were seeded in 12-well or 24-well plates overnight, and transfected with  
384 plasmids using Lipofectamine 2000 (Invitrogen) when they reached 80% confluence. A stable  
385 CtBP1/2 knockdown cell line was generated from RAW264.7 cells by incubating the cells with  
386 CtBP1/2 shRNA lentiviral stocks for 3 hours. Puromycin was added after 48 hours, and infected  
387 cells were selected over 10 passages. Stable clones were pooled for propagation and experiments.

388 Studies were initiated by washing cells into serum-free Dulbecco's minimal essential medium  
389 containing 6 mM glutamine and 2 mM glucose (or no glucose, where indicated).  
390 Lipopolysaccharide (LPS), lactate, and metabolic inhibitors were added to this medium from  
391 concentrated stocks that were pre-adjusted to pH 7.4, and the cultures were replaced in a 37° C,  
392 5% CO<sub>2</sub> incubator. The final LPS concentration was 10 ng / ml in the cell cultures. All experiments  
393 were repeated at least 3 times, using triplicate wells in each experiment.

394

#### 395 *ATP measurements*

396 Cells were washed with ice cold phosphate-buffered saline and extracted with ice cold 0.5%  
397 trichloroacetic acid. The cell lysate pH was adjusted to 7.8 with 1M Tris base. ATP concentration  
398 was determined by a luciferase-linked method (Promega Enlighten ATP kit) using ATP standards.  
399 Values were normalized to protein concentrations as determined by the Bradford assay (Bio-Rad)  
400 in sister culture wells.

401

#### 402 *Lactate and pyruvate assays*

403 RAW264.7 cells were rinsed with ice-cold phosphate-buffered saline, lysed in 0.2 N NaOH, and  
404 aliquots were taken for protein assay. Lactate and pyruvate were measured in pH-neutralized  
405 lysates by enzyme-linked assays as described<sup>12</sup> using standards treated identically.

406

#### 407 *NADH imaging*

408 Real-time changes in cellular (cytoplasmic) NADH content were estimated by measuring  
409 endogenous NADH fluorescence with 360 nm excitation and > 410 nm emission<sup>59</sup>. Fluorescence  
410 images were acquired at 1 minute intervals after 5 minutes of baseline recording. Regions of  
411 interest were selected from the nucleus to eliminate signal from mitochondria, and cytochalasin D  
412 (1 μM) was included to prevent cell movement. Images acquired from each cell were used to  
413 calculate change in fluorescence intensity / average of pre-treatment fluorescence intensity  
414 ( $\Delta F/F_0$ ). In a subset of experiments cells were pre-incubated with 200 nM Mitotracker Red-FM  
415 (Molecular Probes) to verify that the NADH fluorescence measurements were not contaminated  
416 by mitochondrial NADH fluorescence. Mitochondrial and NADH signals were imaged by  
417 interleaving NADH fluorescence excitation and Mitotraker (excitation 550 nm; emission > 610 nm).

418

419 *Nitric oxide measurements*

420 Production of nitric oxide was assessed by analyzing nitrite concentrations in the culture  
421 medium collected after 24 hours incubation under the designated conditions. Aliquots of culture  
422 medium or nitrite standards prepared in culture medium were mixed with equal volumes of Griess  
423 reagent and light absorbance was measured at 540 nm<sup>56</sup>. Values were normalized to the protein  
424 content of each culture well.

425

426 *Luciferase reporter gene assays*

427 Cells were transfected with 300 ng of *5xNF-κB* or *iNOS* firefly luciferase constructs using  
428 Lipofectamine 2000 (Life Technologies), and co-transfected with 100 ng of GL3-Renilla luciferase  
429 construct (Promega) as an internal control of transfection efficiency. In some experiments cells  
430 were also transfected with a CtBP constructs (200 ng) or CtBP empty control vector. Renilla  
431 luciferase and firefly luciferase activity were measured in cell lysates using a dual luciferase assay  
432 kit (Promega) on a Modulus Microplate Reader (Turner Biosystems). Reporter luciferase activity  
433 was normalized to Renilla luciferase activity in each assay.

434

435 *Microarray and differential expression analysis*

436 Cells were harvested after 24 hours incubation under the designated conditions. RNA was  
437 extracted and arrayed in triplicates using Mouse OneArray chip (Phalanx Biotech). Data analysis  
438 was performed using Bioconductor packages in R ([www.bioconductor.org](http://www.bioconductor.org)). Raw reads from  
439 microarrays were first normalized across the samples using the 'vsr' package from Bioconductor  
440<sup>60</sup>. The normalized expression levels of the samples (with technical and experimental duplicates)  
441 were then fitted with a mixed linear model using the 'limma' package from Bioconductor<sup>61</sup>.  
442 Differential expression between pairs of treatment factors were also calculated using the 'limma'  
443 package, and the resulting p-values were adjusted for multiple tests using the Benjamin-Hochberg  
444 procedure. A Venn diagram was also generated to visualize the overlap of differentially expressed  
445 genes between pairs of factors among three factors, using R codes adapted from the 'limma'  
446 package. Shared transcription factor binding sites were identified by blast differentially expressed  
447 genes in the oPOSSUM server (<http://opossum.cisreg.ca/oPOSSUM3/>) with a filter setting of Z-  
448 score above 15.

449

450 *Quantitative real-time PCR analysis*

451 RNA was extracted from freshly harvested cells (Qiagen), treated with DNase I (Promega) and  
452 first-strand cDNA was synthesized from 2 µg total RNA with Oligo (dT) primers (Life Technologies).  
453 Real-time PCR with SYBR green detection (Applied Biosystems) was performed as described  
454 previously<sup>62</sup> using an ABI 7900HT FAST Real-Time PCR System. Dilution series and standard curves  
455 of beta-actin were amplified on each plate for all experiments. Transcript levels of all genes from  
456 each sample were normalized to its β-Actin mRNA level using the  $2^{-\Delta\Delta^{CT}}$  method<sup>62</sup>.

457

458 *Co-immunoprecipitation and western blots*

459 Cells were lysed with M-PER reagent (Pierce) supplemented with benzonase nuclease  
460 (Novagen) and protease inhibitors (Roche). Soluble lysate was centrifuged for 10 minutes at 4°C  
461 and the supernatant was incubated with anti-Flag M2 agarose (Sigma) overnight. The M2 agarose  
462 was washed 5 times with 0.25% Triton X-100 / phosphate-buffered saline and 3 times with 0.5%  
463 Triton X-100 / phosphate-buffered saline. Bound protein was eluted using 1X Sample Loading  
464 Buffer (Invitrogen) and heated to 100°C for 5 minutes. Lysate and eluate were resolved on 10%  
465 SDS-PAGE gels, and transferred to PVDF membranes (Millipore)<sup>62</sup>. The blots were probed with  
466 mouse polyclonal anti iNOS (Upstate, #06-573; 1:1000), rabbit polyclonal anti β-actin (Sigma-  
467 Aldrich, #A2066; 1:1000), and mouse monoclonal anti-CtBP (AbNova, # H1487-MO1, 1:1000).

468

469 *Chromatin immunoprecipitation*

470 Cells were treated with 1% formaldehyde for 10 minutes at 37°C and rinsed twice with ice-  
471 cold phosphate-buffered saline supplemented with phenylmethanesulfonyl fluoride and protease  
472 inhibitors (Roche). Cells were then lysed, sonicated on ice, and centrifuged. Aliquots of the  
473 supernatants were heated to reverse crosslinks and recover genomic DNA for an input control. A  
474 ChIP assay kit (Millipore) was used with mouse antibody to CtBP (AbNova, # H1487-MO1, 1:250  
475 dilution) and rabbit antibodies to p300, HDAC1, and p65 (Santa Cruz Biotechnology; sc-585, sc-  
476 7872, sc-372) or acetyl H3 (Cell Signaling, #8173), each at 1:250 dilutions, and with mouse and  
477 rabbit IgG controls (Cell Signaling). Precipitated material was eluted by two 15 minute incubations  
478 at room temperature with 250 µl of 1% SDS / 0.1 M NaHCO<sub>3</sub>. Chromatin was crosslink-reversed  
479 and submitted to RNase and proteinase K digestion. DNA was extracted by phenol-chloroform and

480 the DNA from both the CHIP and the input controls were analyzed by quantitative real-time PCR  
481 analysis. Primers targeting the iNOS, Il-1b, and Il6 promoter regions were as published<sup>63, 64</sup>.

482

### 483 *Peptide design and synthesis*

484 The crystal structure of a rat CtBP dimer complexed with NAD(H) (PDB 1HKU)<sup>37</sup> using Accelrys  
485 DS Viewer 1.7 suggested that a peptide near the center of the dimerization region, if stably folded,  
486 might interfere with dimer formation. This dimerization region contains two alpha helical domains  
487 that are structurally conserved in CtBP family members and also contains residues that, when  
488 mutated, prevent dimerization of drosophila CtBP<sup>22</sup>. A corresponding CtBP peptide along with a  
489 control peptide lacking any known cell function were generated and fused to an N-terminal Tat  
490 sequence by CPC Scientific (Sunnyvale, CA). The CtBP peptide sequence was  
491 GRKKRRQRRRCVEETADSTLCHILNLYRRTTWLHQALREG (with the Tat sequence underlined), and the  
492 control peptide sequence was GRKKRRQRRRCSFNSYELGSLCYGRKKRRQRR.

493

### 494 *CtBP dimerization assay*

495 CtBP1-HA and CtBP1-Flag expression constructs were generated by PCR amplification of full  
496 length CtBP1 coding sequence from mouse brain-derived cDNA, followed by cloning in-frame into  
497 pSelect-CHA-zeo (Invivogen, San Diego, CA) and pCMV-(DYKDDDDK)-C (Clontech, Mountain View,  
498 CA) vectors, respectively. Clone identity and integrity were verified by sequence analysis. COS-7  
499 cells were grown to 75% confluence in 6-well plates in Dulbecco's minimal essential medium  
500 containing fetal bovine serum and 230  $\mu$ M sodium pyruvate. 5  $\mu$ g of each plasmid per plate was  
501 transfected using Lipofectamine2000 (Life Technologies, Inc., Grand Island, NY). 24 hours post  
502 transfection, cells were washed once in 1 x PBS and lysed in NP-40 buffer (20 mM Tris HCl pH 8.0,  
503 137 mM NaCl, 10% glycerol, 1% Nonidet P-40, 2mM EDTA) containing Complete Mini protease  
504 inhibitor cocktail (Roche, Indianapolis, IN). Lysates were cleared of cellular debris by brief  
505 centrifugation and concentration determined by Pierce BCA Protein Assay (Thermo Scientific,  
506 Rockford, IL). Forty  $\mu$ g protein from each sample lysate was incubated at 37<sup>o</sup> C for 20 minutes  
507 either with or without the addition of 50  $\mu$ M CtBP peptide. In some studies incubation solution  
508 also contained 10 mM sodium lactate and 10  $\mu$ M NADH to promote CtBP dimerization. Co-  
509 immunoprecipitation was performed by overnight incubation of samples with 2  $\mu$ g mouse  
510 monoclonal ANTI-FLAG M2 antibody (Sigma-Aldrich, # F3165), 3hr incubation with 40  $\mu$ L

511    prewashed protein A/G-Sepharose beads (Biovision Inc., Milpitas, CA) and serially washed with NP-  
512    40 buffer per manufacturer’s instructions. Bound protein was eluted from Sepharose beads by  
513    addition of NuPAGE LDS Sample buffer (Life Technologies, Inc.) and analyzed by standard SDS-  
514    PAGE gel electrophoresis using polyclonal rabbit anti-HA antibody (Thermo Scientific, # PA1-985,  
515    1:500 dilution).

516

517    *Statistical analyses.*

518            In all cell culture or slice culture studies the ‘n’ values denote the number of independent  
519    experiments, each using neurons prepared from different mice. Each independent experiment  
520    contained triplicate culture wells. Data other than the microarray results are expressed as means  $\pm$   
521    SEM and assessed using one-way ANOVA followed by either the Tukey–Kramer test where  
522    multiple groups are compared against one another, or Dunnett’s test where multiple groups are  
523    compared against a common control group. All data analyses were performed while blinded to the  
524    treatment conditions.

525

526            *Data availability*

527            The microarray data have been deposited in the FigShare database at  
528    <https://doi.org/10.6084/m9.figshare.c.3828235.v1>. The authors declare that all other relevant  
529    data supporting the findings of the study are available in this article and its Supplementary  
530    Information files, or from the corresponding author upon request.

531 **References**

- 532 1. Brown GC, Neher JJ. Inflammatory neurodegeneration and mechanisms of microglial killing  
533 of neurons. *Mol Neurobiol* **41**, 242-247 (2010).
- 534 2. Chen Y, Won SJ, Xu Y, Swanson RA. Targeting Microglial Activation in Stroke Therapy:  
535 Pharmacological Tools and Gender Effects. *Curr Med Chem* **21**, 2146-2155 (2014).
- 536 3. An C, *et al.* Molecular dialogs between the ischemic brain and the peripheral immune  
537 system: dualistic roles in injury and repair. *Prog Neurobiol* **115**, 6-24 (2014).
- 538 4. Loane DJ, Byrnes KR. Role of microglia in neurotrauma. *Neurotherapeutics* **7**, 366-377  
539 (2010).
- 540 5. Longo VD, Mattson MP. Fasting: molecular mechanisms and clinical applications. *Cell*  
541 *Metab* **19**, 181-192 (2014).
- 542 6. Goth A. Inhibition of anaphylactoid edema in the rat by 2-deoxyglucose. *Am J Physiol* **197**,  
543 1056-1058 (1959).
- 544 7. Gasior M, Rogawski MA, Hartman AL. Neuroprotective and disease-modifying effects of the  
545 ketogenic diet. *Behav Pharmacol* **17**, 431-439 (2006).
- 546 8. Yu ZF, Mattson MP. Dietary restriction and 2-deoxyglucose administration reduce focal  
547 ischemic brain damage and improve behavioral outcome: evidence for a preconditioning  
548 mechanism. *J Neurosci Res* **57**, 830-839 (1999).
- 549 9. Loncarevic-Vasiljkovic N, *et al.* Caloric restriction suppresses microglial activation and  
550 prevents neuroapoptosis following cortical injury in rats. *PLoS One* **7**, e37215 (2012).
- 551 10. Tu YF, Lu PJ, Huang CC, Ho CJ, Chou YP. Moderate dietary restriction reduces p53-mediated  
552 neurovascular damage and microglia activation after hypoxic ischemia in neonatal brain.  
553 *Stroke* **43**, 491-498 (2012).
- 554 11. Appelberg KS, Hovda DA, Prins ML. The effects of a ketogenic diet on behavioral outcome  
555 after controlled cortical impact injury in the juvenile and adult rat. *J Neurotrauma* **26**, 497-  
556 506 (2009).
- 557 12. Wang Q, *et al.* Pyruvate protects against experimental stroke via an anti-inflammatory  
558 mechanism. *Neurobiol Dis* **36**, 223-231 (2009).

- 559 13. Kaur C, Rathnasamy G, Ling EA. Roles of activated microglia in hypoxia induced  
560 neuroinflammation in the developing brain and the retina. *J Neuroimmune Pharmacol* **8**,  
561 66-78 (2012).
- 562 14. Robbins NM, Swanson RA. Opposing effects of glucose on stroke and reperfusion injury:  
563 acidosis, oxidative stress, and energy metabolism. *Stroke* **45**, 1881-1886 (2014).
- 564 15. Hotamisligil GS. Inflammation and metabolic disorders. *Nature* **444**, 860-867 (2006).
- 565 16. Ghosh S, George S, Roy U, Ramachandran D, Kolthur-Seetharam U. NAD: a master regulator  
566 of transcription. *Biochim Biophys Acta* **1799**, 681-693 (2010).
- 567 17. Hildebrand JD, Soriano P. Overlapping and unique roles for C-terminal binding protein 1  
568 (CtBP1) and CtBP2 during mouse development. *Mol Cell Biol* **22**, 5296-5307 (2002).
- 569 18. Chinnadurai G. Transcriptional regulation by C-terminal binding proteins. *Int J Biochem Cell*  
570 *Biol* **39**, 1593-1607 (2007).
- 571 19. Kuppuswamy M, *et al.* Role of the PLDLS-binding cleft region of CtBP1 in recruitment of  
572 core and auxiliary components of the corepressor complex. *Mol Cell Biol* **28**, 269-281  
573 (2008).
- 574 20. Kim JH, Cho EJ, Kim ST, Youn HD. CtBP represses p300-mediated transcriptional activation  
575 by direct association with its bromodomain. *Nat Struct Mol Biol* **12**, 423-428 (2005).
- 576 21. Birts CN, *et al.* A cyclic peptide inhibitor of C-terminal binding protein dimerization links  
577 metabolism with mitotic fidelity in breast cancer cells. *Chem Sci* **4**, 3046-3057 (2013).
- 578 22. Bhambhani C, Chang JL, Akey DL, Cadigan KM. The oligomeric state of CtBP determines its  
579 role as a transcriptional co-activator and co-repressor of Wingless targets. *EMBO J* **30**,  
580 2031-2043 (2011).
- 581 23. Verger A, *et al.* Mechanisms directing the nuclear localization of the CtBP family proteins.  
582 *Mol Cell Biol* **26**, 4882-4894 (2006).
- 583 24. Quinlan KG, *et al.* Role of the C-terminal binding protein PXDLS motif binding cleft in  
584 protein interactions and transcriptional repression. *Mol Cell Biol* **26**, 8202-8213 (2006).
- 585 25. Chen LF, Mu Y, Greene WC. Acetylation of RelA at discrete sites regulates distinct nuclear  
586 functions of NF-kappaB. *EMBO J* **21**, 6539-6548 (2002).
- 587 26. Zhang Q, Piston DW, Goodman RH. Regulation of corepressor function by nuclear NADH.  
588 *Science* **295**, 1895-1897 (2002).

- 589 27. Garriga-Canut M, *et al.* 2-Deoxy-D-glucose reduces epilepsy progression by NRSF-CtBP-  
590 dependent metabolic regulation of chromatin structure. *Nat Neurosci* **9**, 1382-1387 (2006).
- 591 28. Yao J, Chen S, Mao Z, Cadenas E, Brinton RD. 2-Deoxy-D-glucose treatment induces  
592 ketogenesis, sustains mitochondrial function, and reduces pathology in female mouse  
593 model of Alzheimer's disease. *PLoS One* **6**, e21788 (2011).
- 594 29. Forstermann U, Kleinert H. Nitric oxide synthase: expression and expressional control of  
595 the three isoforms. *Naunyn Schmiedebergs Arch Pharmacol* **352**, 351-364 (1995).
- 596 30. Williamson DH, Lund P, Krebs HA. The redox state of free nicotinamide-adenine  
597 dinucleotide in the cytoplasm and mitochondria of rat liver. *Biochem J* **103**, 514-527 (1967).
- 598 31. Alano CC, Tran A, Tao R, Ying W, Karliner JS, Swanson RA. Differences among cell types in  
599 NAD(+) compartmentalization: A comparison of neurons, astrocytes, and cardiac myocytes.  
600 *J Neurosci Res* **85**, 3378-3385 (2007).
- 601 32. Karovic O, *et al.* Toxic effects of cobalt in primary cultures of mouse astrocytes. Similarities  
602 with hypoxia and role of HIF-1alpha. *Biochem Pharmacol* **73**, 694-708 (2007).
- 603 33. Poole RC, Halestrap AP. Transport of lactate and other monocarboxylates across  
604 mammalian plasma membranes. *Am J Physiol* **264**, C761-782 (1993).
- 605 34. Reiss PD, Zuurendonk PF, Veech RL. Measurement of tissue purine, pyrimidine, and other  
606 nucleotides by radial compression high-performance liquid chromatography. *Anal Biochem*  
607 **140**, 162-171 (1984).
- 608 35. Ying W. NAD<sup>+</sup>/NADH and NADP<sup>+</sup>/NADPH in cellular functions and cell death: regulation  
609 and biological consequences. *Antioxid Redox Signal* **10**, 179-206 (2008).
- 610 36. Palero JA, Bader AN, de Bruijn HS, der Ploeg van den Heuvel A, Sterenborg HJ, Gerritsen  
611 HC. In vivo monitoring of protein-bound and free NADH during ischemia by nonlinear  
612 spectral imaging microscopy. *Biomed Opt Express* **2**, 1030-1039 (2011).
- 613 37. Nardini M, *et al.* CtBP/BARS: a dual-function protein involved in transcription co-repression  
614 and Golgi membrane fission. *EMBO J* **22**, 3122-3130 (2003).
- 615 38. Qin H, *et al.* Signal transducer and activator of transcription-3/suppressor of cytokine  
616 signaling-3 (STAT3/SOCS3) axis in myeloid cells regulates neuroinflammation. *Proc Natl*  
617 *Acad Sci U S A* **109**, 5004-5009 (2012).
- 618 39. Meloni AR, Lai CH, Yao TP, Nevins JR. A mechanism of COOH-terminal binding protein-  
619 mediated repression. *Mol Cancer Res* **3**, 575-583 (2005).

- 620 40. Di LJ, Fernandez AG, De Siervi A, Longo DL, Gardner K. Transcriptional regulation of BRCA1  
621 expression by a metabolic switch. *Nat Struct Mol Biol* **17**, 1406-1413 (2011).
- 622 41. Zhang Q, Wang SY, Nottke AC, Rocheleau JV, Piston DW, Goodman RH. Redox sensor CtBP  
623 mediates hypoxia-induced tumor cell migration. *Proc Natl Acad Sci U S A* **103**, 9029-9033  
624 (2006).
- 625 42. Fjeld CC, Birdsong WT, Goodman RH. Differential binding of NAD<sup>+</sup> and NADH allows the  
626 transcriptional corepressor carboxyl-terminal binding protein to serve as a metabolic  
627 sensor. *Proc Natl Acad Sci U S A* **100**, 9202-9207 (2003).
- 628 43. McGettrick AF, O'Neill LA. How metabolism generates signals during innate immunity and  
629 inflammation. *J Biol Chem* **288**, 22893-22898 (2013).
- 630 44. Feldman JL, Dittenhafer-Reed KE, Denu JM. Sirtuin catalysis and regulation. *J Biol Chem*  
631 **287**, 42419-42427 (2012).
- 632 45. Bergman LM, Morris L, Darley M, Mirnezami AH, Gunatilake SC, Blaydes JP. Role of the  
633 unique N-terminal domain of CtBP2 in determining the subcellular localisation of CtBP  
634 family proteins. *BMC Cell Biol* **7**, 35 (2006).
- 635 46. Saijo K, Collier JG, Li AC, Katzenellenbogen JA, Glass CK. An ADIOL-ERbeta-CtBP  
636 transrepression pathway negatively regulates microglia-mediated inflammation. *Cell* **145**,  
637 584-595 (2011).
- 638 47. Xu X, *et al.* EVI1 acts as an inducible negative-feedback regulator of NF-kappaB by inhibiting  
639 p65 acetylation. *J Immunol* **188**, 6371-6380 (2012).
- 640 48. Moon JS, *et al.* mTORC1-Induced HK1-Dependent Glycolysis Regulates NLRP3  
641 Inflammasome Activation. *Cell Rep* **12**, 102-115 (2015).
- 642 49. Wang B, *et al.* Glycolysis-dependent histone deacetylase 4 degradation regulates  
643 inflammatory cytokine production. *Mol Biol Cell* **25**, 3300-3307 (2015).
- 644 50. Manigrasso MB, Juranek J, Ramasamy R, Schmidt AM. Unlocking the biology of RAGE in  
645 diabetic microvascular complications. *Trends Endocrinol Metab* **25**, 15-22 (2014).
- 646 51. Warburg O. On respiratory impairment in cancer cells. *Science* **124**, 269-270 (1956).
- 647 52. Calle MC, Fernandez ML. Inflammation and type 2 diabetes. *Diabetes Metab* **38**, 183-191  
648 (2012).

- 649 53. Horvath P, Oliver SR, Ganesan G, Zaldivar FP, Jr., Radom-Aizik S, Galassetti PR. Fasting  
650 glucose level modulates cell surface expression of CD11b and CD66b in granulocytes and  
651 monocytes of patients with type 2 diabetes. *J Investig Med* **61**, 972-977 (2013).
- 652 54. Lowenstein CJ, *et al.* Macrophage nitric oxide synthase gene: two upstream regions  
653 mediate induction by interferon gamma and lipopolysaccharide. *Proc Natl Acad Sci U S A*  
654 **90**, 9730-9734 (1993).
- 655 55. Suh SW, *et al.* Glucose and NADPH oxidase drive neuronal superoxide formation in stroke.  
656 *Ann Neurol* **64**, 654-663 (2008).
- 657 56. Kauppinen TM, Higashi Y, Suh SW, Escartin C, Nagasawa K, Swanson RA. Zinc triggers  
658 microglial activation. *J Neurosci* **28**, 5827-5835 (2008).
- 659 57. d'Avila JC, *et al.* Microglial activation induced by brain trauma is suppressed by post-injury  
660 treatment with a PARP inhibitor. *Journal of neuroinflammation* **9**, 31 (2012).
- 661 58. del Rio JA, Soriano E. Regenerating cortical connections in a dish: the entorhino-  
662 hippocampal organotypic slice co-culture as tool for pharmacological screening of  
663 molecules promoting axon regeneration. *Nat Protoc* **5**, 217-226 (2010).
- 664 59. Brennan AM, Connor JA, Shuttleworth CW. NAD(P)H fluorescence transients after synaptic  
665 activity in brain slices: predominant role of mitochondrial function. *J Cereb Blood Flow*  
666 *Metab* **26**, 1389-1406 (2006).
- 667 60. Huber W, von Heydebreck A, Sultmann H, Poustka A, Vingron M. Variance stabilization  
668 applied to microarray data calibration and to the quantification of differential expression.  
669 *Bioinformatics* **18 Suppl 1**, S96-104 (2002).
- 670 61. Smyth GK. Linear models and empirical bayes methods for assessing differential expression  
671 in microarray experiments. *Stat Appl Genet Mol Biol* **3**, Article3 (2004).
- 672 62. Shen Y, *et al.* Mutations in PNKD causing paroxysmal dyskinesia alters protein cleavage and  
673 stability. *Hum Mol Genet* **20**, 2322-2332 (2011).
- 674 63. Saijo K, *et al.* A Nurr1/CoREST pathway in microglia and astrocytes protects dopaminergic  
675 neurons from inflammation-induced death. *Cell* **137**, 47-59 (2009).
- 676 64. Zschiegler I, *et al.* Coactivator function of RIP140 for NFkappaB/RelA-dependent cytokine  
677 gene expression. *Blood* **112**, 264-276 (2008).
- 678
- 679

680

681 **Acknowledgements**

682 We thank J. Blaydes for the CtBP2 G189A plasmid, C. Lowenstein for the *iNOS* promoter-  
683 luciferase reporter, W. Sellers for the p300 plasmid, W. Greene for the p65 plasmid, and A. Roopra  
684 for the FLAG-tagged CtBP2 plasmid, the *CtBP1,2<sup>-/-</sup>* MEF cell lines, and constructive discussions. This  
685 work was supported by the NIH (NS041421) and the Dept. of Veterans Affairs.

686

687

688 **Author Contributions**

689 Y.S. and R.A.S. conceived the project. Y.S., D.K., A.M.B-M., and R.A.S. designed the  
690 experiments; Y.S., D.K., J-E.K., L.H.L. and Y.C. evaluated inflammatory responses, CtBP expression,  
691 and performed CtBP immunoprecipitation studies in the cell cultures; A.M.B-M. performed the  
692 fluorescence NADH analyses and ATP measurements; Y. S. and Y.H. provided data analysis of the  
693 microarray and promoter enrichment studies; S.J.W. performed the in vivo studies; S.M.M.  
694 designed the CtBP peptide; D.K. established and performed the dimerization assay with the CtBP  
695 peptide; and Y.S., D.K., and R.A.S wrote the manuscript.

696

697

698 **Competing Financial Interests**

699 The authors declare no competing financial interests.

700

701 **FIGURE LEGENDS**

702 **Figure 1. 2-deoxyglucose suppresses LPS-induced microglial activation.**

703 (A) Immunostaining for CD11b identifies activated microglia in rat hippocampus. CD11b expression  
704 was increased 24 hours after intraperitoneal injection with LPS (10 mg / kg). The increase was  
705 attenuated by co-injection with 2-deoxyglucose (2DG; 100mg / kg). Scale bar = 100  $\mu$ m. \*\* p <  
706 0.01, n = 6. (B) Immunostaining for Iba1 and iNOS identify activated microglia in mouse  
707 hippocampal slice cultures after 24 hours incubation with LPS (10  $\mu$ g / ml) or LPS +2DG (1 mM).  
708 Scale bar = 100  $\mu$ m; n  $\geq$  3, \* p < 0.05. Culture medium contained 6 mM glutamine and 5 mM  
709 glucose. (C) Effects of 1mM 2DG on LPS (10 ng / ml) - induced iNOS transcript and protein  
710 expression in primary microglial cultures. n = 5; \* p < 0.05, \*\* p < 0.01. Full length immunoblots  
711 are shown in Supplementary Fig. 3. (D,E). Effects of 1 mM 2DG on LPS -induced iNOS protein  
712 expression, mRNA expression, and nitric oxide production in cultured RAW267.4 cells. n  $\geq$  3; \*p <  
713 0.05, \*\*p < 0.01. (F) Relative ATP levels measured after 24 hours incubation in control medium, 1  
714 mM 2-deoxyglucose, 200  $\mu$ M CoCl<sub>2</sub>, 20 mM lactate, glucose free medium, or in 2  $\mu$ M  
715 trifluorocarbonylcyanide phenylhydrazide (FCCP) as a positive control. n = 4; \*\* p < 0.01 v.  
716 control. Error bars show s.e.m.

717

718 **Figure 2. Relationships between glucose metabolism and cytosolic NADH:NAD<sup>+</sup> ratio.**

719 (A) Factors that reduce glucose flux through glycolysis, such as reduced glucose availability or  
720 glycolytic inhibitors, reduce NADH levels and thereby reduce NADH:NAD<sup>+</sup> ratio, whereas factors  
721 that inhibit oxidative metabolism, such as hypoxia and mitochondrial inhibitors, have the opposite  
722 effect. Glutamine provides ketone bodies ( $\alpha$ -ketoglutarate) to fuel mitochondrial ATP production  
723 in the absence of glycolysis. Lactate dehydrogenase (LDH) maintains the lactate:pyruvate ratio in  
724 equilibrium with the cytosolic NADH:NAD<sup>+</sup> ratio. (B) The lactate:pyruvate ratio provides an index  
725 of the cytosolic NADH:NAD<sup>+</sup> ratio in cells treated with glycolytic and mitochondrial inhibitors. 2DG,  
726 1 mM 2-deoxyglucose; 0 Glu, glucose-free medium; CoCl<sub>2</sub>, 200  $\mu$ M cobalt chloride; antimycin, 1  
727  $\mu$ M antimycin A. n = 4; \*p < 0.05 v. control. (C) LPS-induced iNOS expression was suppressed in  
728 RAW267.4 cells treated with 1 mM 2DG or glucose-free medium, and increased in cells treated  
729 with the mitochondrial inhibitor cobalt chloride (CoCl<sub>2</sub>, 200  $\mu$ M ). n = 4; \* p < 0.05 v. control. Error  
730 bars show s.e.m. Full length immunoblots are shown in Supplementary Fig. 3.

731

732 **Figure 3. Lactate reverses the effects of glycolytic inhibition on both cytosolic NADH levels and**  
733 **LPS-induced iNOS expression.**

734 (A,B) The effects of glucose-free medium and 2DG on LPS-induced iNOS expression are reversed by  
735 20 mM lactate.  $n \geq 3$ ,  $*p < 0.05$ . Full length immunoblots are shown in Supplementary Fig. 3. (C)  
736 The effects of glucose-free medium and 2DG on LPS-induced *iNOS* transcription are reversed by 20  
737 mM lactate, as measured by relative light units (RLU) emitted by a cells transfected with a  
738 luciferase-coupled *iNOS* reporter gene.  $n = 3$ ;  $*p < 0.05$ . (D) Effects of lactate on cytosolic  
739 NAD(P)H levels as measured by intrinsic fluorescence (blue). Mitochondria are labeled with  
740 Mitotracker (red). Lower row images are enlarged views of areas defined by rectangle in upper  
741 row. Boxes in lower row identify a mitochondria-rich peri-nuclear region and a mitochondria-free  
742 nuclear region in one cell. (E) Example of real-time NAD(P)H fluorescence changes recorded from  
743 these two regions during incubation with 1 mM 2-deoxyglucose (added at arrow). (F) Quantified  
744 results showing relative cytosolic NAD(P)H fluorescence changes induced by incubation with 1 mM  
745 2-deoxyglucose  $\pm$  20 mM lactate, glucose-free medium  $\pm$  20 mM lactate, 20 mM lactate, 200  $\mu$ M  
746 cobalt chloride, or 1  $\mu$ M antimycin A.  $n = 5$ ;  $*p < 0.01$ ,  $^{\#}p < 0.01$  v. control. Error bars show s.e.m.  
747

748 **Figure 4. LPS and 2-deoxyglucose influence NF- $\kappa$ B – mediated gene transcription.**

749 (A) Microarray analysis identified 994 genes differentially regulated by LPS (red) and 781 genes by  
750 (2DG+LPS) (blue), relative to control conditions. 579 of LPS-response genes were affected by co-  
751 incubation with 2DG. (B) RT-PCR measures of NF- $\kappa$ B –driven pro-inflammatory cytokines  
752 confirmed that LPS-induced induction was attenuated by 2DG. *IL-1b*, interleukin-1beta; *IL-6*,  
753 interleukin-6.  $n \geq 3$ ;  $*p < 0.05$ ,  $**p < 0.01$ . Error bars show s.e.m.  
754

755 **Figure 5. Knockdown of CtBP eliminates the effects of 2DG and glucose-free medium.**

756 (A) Representative western blot showing reduced expression of CtBP1/2 protein in RAW264.7 cells  
757 transfected with shRNA targeting CtBP1 and CtBP2 (CtBP KD). Full length immunoblots are shown  
758 in Supplementary Fig. 3. (B,C) shRNA knockdown of CtBP1/2 negates the effect of both 2DG and  
759 glucose-free medium on LPS-induced iNOS expression and nitric oxide production. Results for wild-  
760 type (WT) cells were normalized to control (no LPS) WT cells, and results for CtBP knockdown cells  
761 (CtBP KD) were normalized to control CtBP KD cells.  $n = 4$ ;  $*p < 0.05$ ; ns, not significant. Error bars  
762 show S.E.M. (D) Knockdown of CtBP1/2 negates the effects of 2DG on LPS-induced NF- $\kappa$ B  
763 reporter gene activation.  $n \geq 3$ ;  $*p < 0.05$ ; ns, not significant. Error bars show s.e.m. (E) 2DG did

764 not suppress LPS-induced transcription of *iNOS*, *Il-1b*, or *IL-6* in the CtBP KD cells. n = 3. (Compare  
765 to Figs. 1D, 4B).

766

767 **Figure 6. The NAD(H) binding site on CtBP is required for its effect on inflammatory responses.**

768 (A) Transfection with CtBP1, CtBP2, and G1892 CtBP2 produced comparable expression levels in  
769 CtBP1<sup>-/-</sup>/CtBP2<sup>-/-</sup> MEF cells. Full length immunoblots are shown in Supplementary Fig. 3. (B-D) MEF  
770 cells were transfected with WT CtBP1, CtBP2 and G189A CtBP2, and additionally transfected with  
771 p65 to induce NF-κB activation. All 3 CtBP constructs suppress *iNOS* and *NF-κB* reporter gene  
772 transcriptional activity, and have no effect on a scrambled-sequence driven luciferase reporter  
773 gene. n = 3; \*p < 0.05 v. empty vector. (E) The mitochondrial inhibitor CoCl<sub>2</sub> increased *NF-κB*  
774 reporter gene activity in cells expressing WT CtBP2 but not in cells expressing G189A CtBP2.  
775 Results are normalized to the increase produced by CoCl<sub>2</sub> in the cells transfected with empty  
776 vector alone. n = 4; \*p < 0.05. (F) Immunostaining in primary microglia shows LPS-induced iNOS  
777 expression is potentiated by CoCl<sub>2</sub> in cells transfected with WT CtBP2, but not G189A CtBP. Larger  
778 nuclei in the images belong to the astrocyte feeder layer. Results are normalized to the increase  
779 produced by 200 μM CoCl<sub>2</sub> in the empty vector - transfected cells. n = 4; \*\*p < 0.01. Error bars  
780 show s.e.m.

781

782 **Figure 7. Direct inhibition of CtBP dimerization blocks LPS-induced pro-inflammatory gene**  
783 **expression.**

784 (A) Schematic of CtBP1 protein showing functional domains and alignment with the CtBP peptide  
785 used to block CtBP dimerization. PLDLS indicates substrate binding domain. The CtBP blocking  
786 peptide includes an N-terminal TAT sequence for cellular internalization. (B) Immunoprecipitation  
787 assay showing ability of CtBP peptide (50 μM) to block dimerization of tagged CtBP proteins  
788 incubated with 10 mM lactate + 10 μM NADH. Full length immunoblots are shown in  
789 Supplementary Fig. 3. Immunoprecipitation was performed with anti-Flag antibody, and CtBP1-  
790 Flag/CtBP1-HA heterodimers were detected by western blots using anti-HA antibody. Lysate  
791 control lane = 5% of input used in immunoprecipitated samples. n = 4. \*\*p < 0.01. (C) CtBP peptide  
792 (5 μM) blocks LPS-induced mRNA expression of pro-inflammatory genes (*iNOS*, *IL-1b* and *IL-6*) in  
793 cultured primary microglia. Ctrl PEP = control peptide. n ≥ 3; \*\*p < 0.01. (D) 2DG blocks LPS-  
794 induced *iNOS* gene expression in microglia isolated from mice after LPS (8 μg) injection into

795 striatum. n = 3-5 per group. \*\*p < 0.01. (E,F) CtBP peptide blocks LPS-induced iNOS expression but  
796 not Socs3 expression in brain microglia. n = 4 per group. \*\*p < 0.01. Error bars show s.e.m.

797

798 **Figure 8. CtBP effects on p300 and NF-κB acetylation**

799 (A) Chromatin immunoprecipitation (ChIP) with antibody to HDAC1, acetyl-H3, and p65 was  
800 performed in RAW264.7 cells to evaluate binding to the IL-6 promoter regions. LPS increased all  
801 three signals, but only the effect of p65 binding was reversed by 2DG (conditions as in Fig. 1C); n =  
802 3, \*p < 0.05. (B) Western blots show LPS-induced p65 acetylation is suppressed by 2DG  
803 (conditions as in Fig. 1C); n = 3, \*p < 0.05. Full length immunoblots are shown in Supplementary  
804 Fig. 3. (C) ChIP was performed to evaluate p300 binding to NF-κB p65 binding sites on promoter  
805 regions of pro-inflammatory cytokines. p300 binding was increased by LPS, and this effect was  
806 attenuated by 2DG (conditions as in Fig. 1C); n = 3, \*p < 0.05. (D) HEK293 cells were transfected  
807 with FLAG-tagged wild-type CtBP2 or G189A CtBP2. Immunoprecipitation using antibody to FLAG  
808 recovered p300 protein, while antibody to IgG, used as a negative control, did not.  
809 Immunoprecipitates from transfected cells treated with 2DG or CoCl<sub>2</sub> for 30 minutes showed  
810 reduced p300 binding to wt CtBP2, but not G189A CtBP2, in cells treated with CoCl<sub>2</sub>. (E) Quantified  
811 results of the immunoprecipitation studies. Results were normalized to p300 in the lysate input. n  
812 = 3; \*, p < 0.05. Error bars show s.e.m.

Figure 1

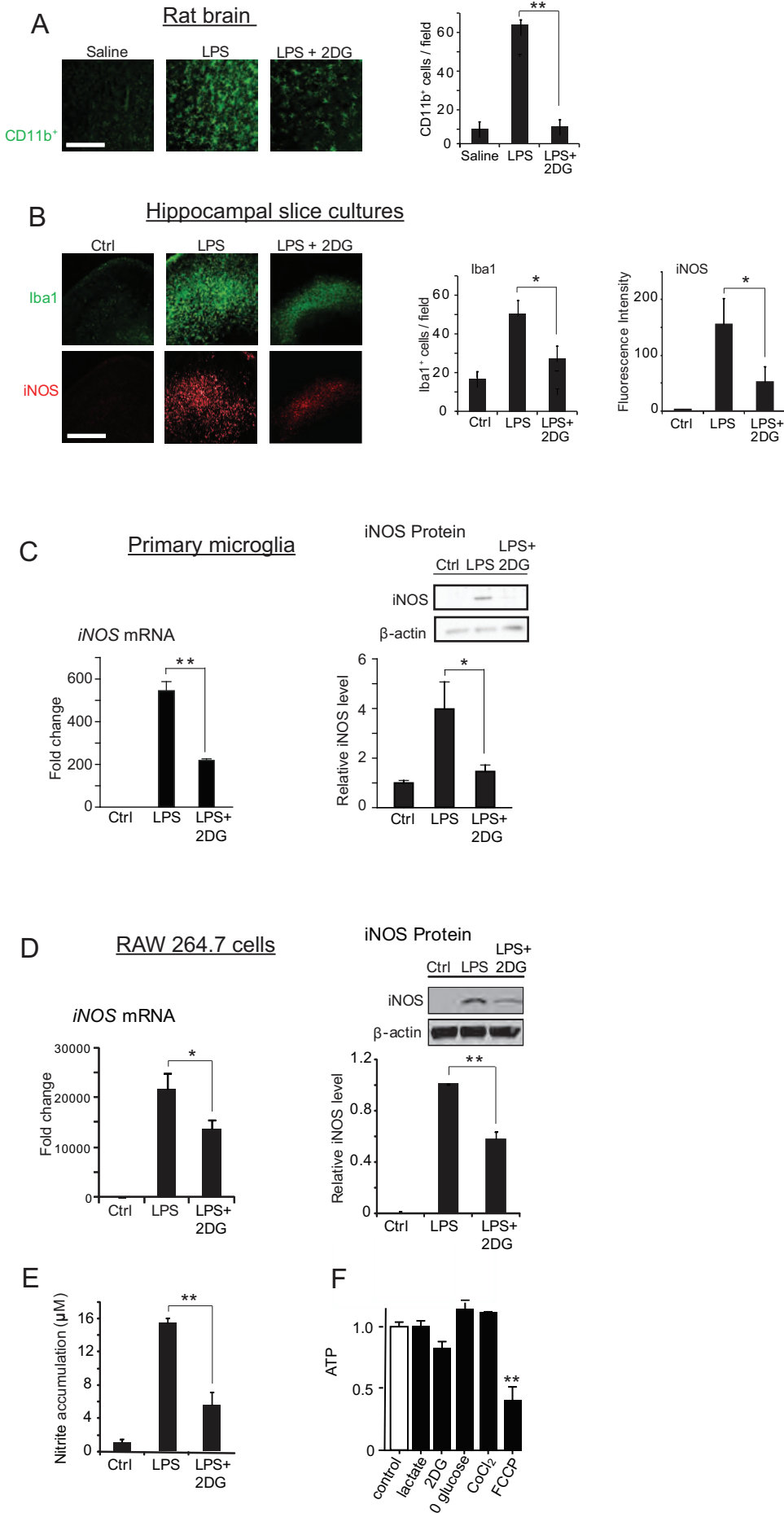
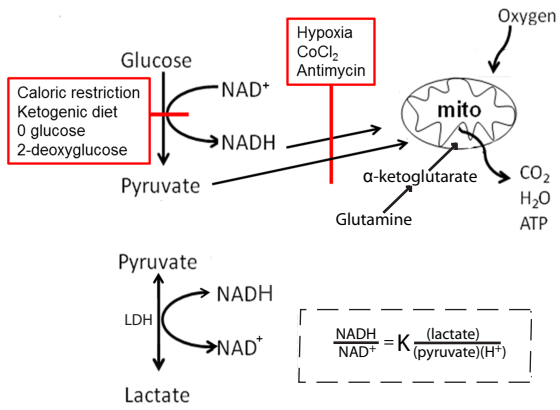
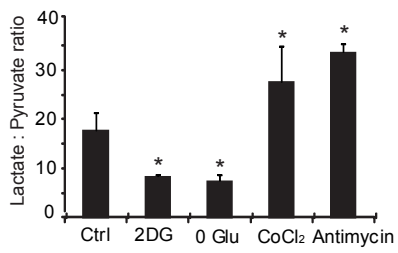


Figure 2

A



B



C

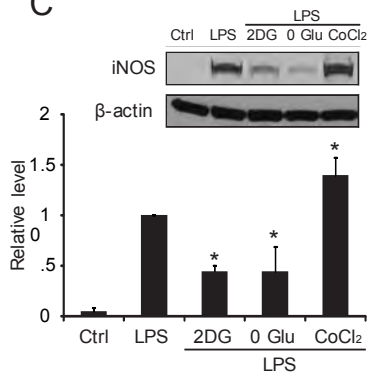


Figure 3

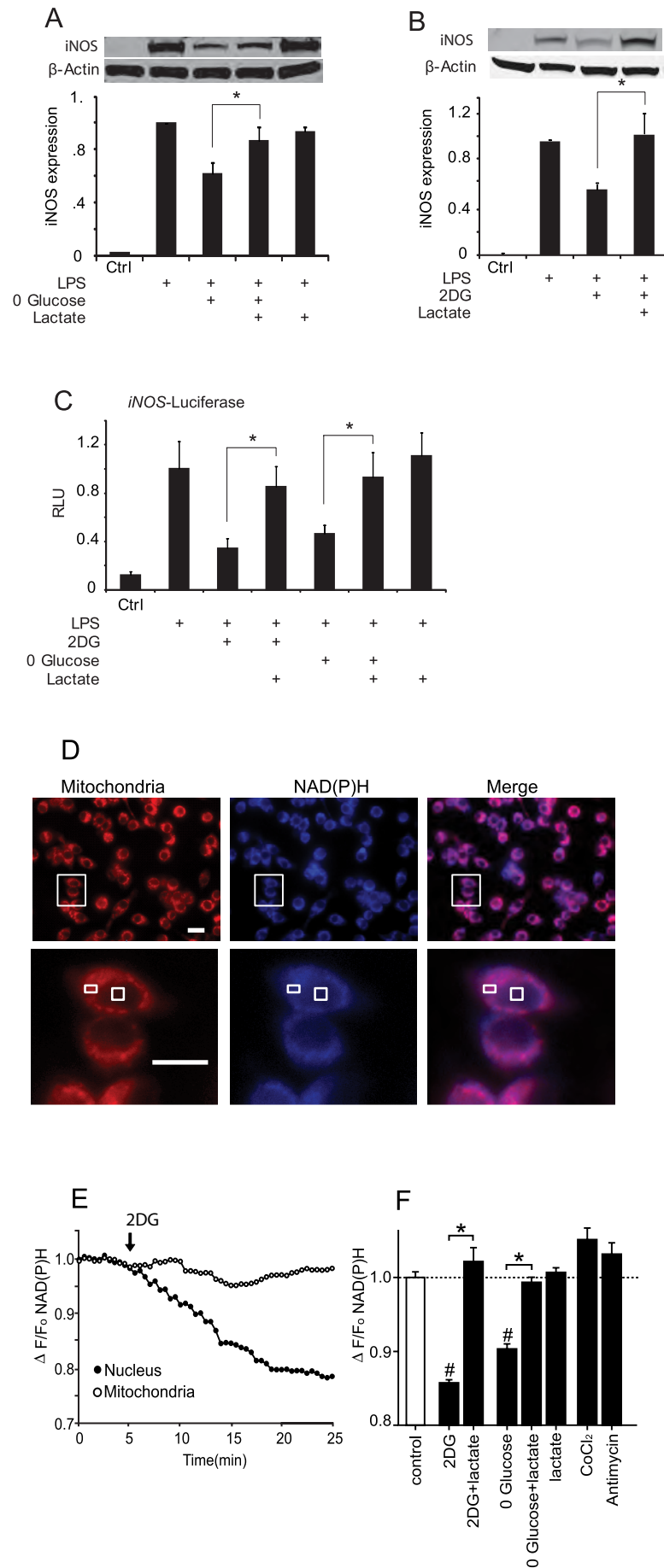


Figure 4

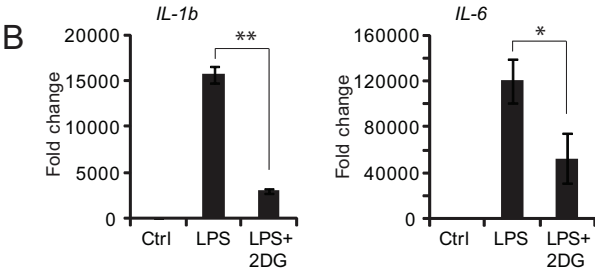
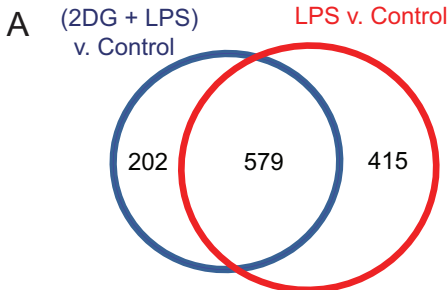


Figure 5

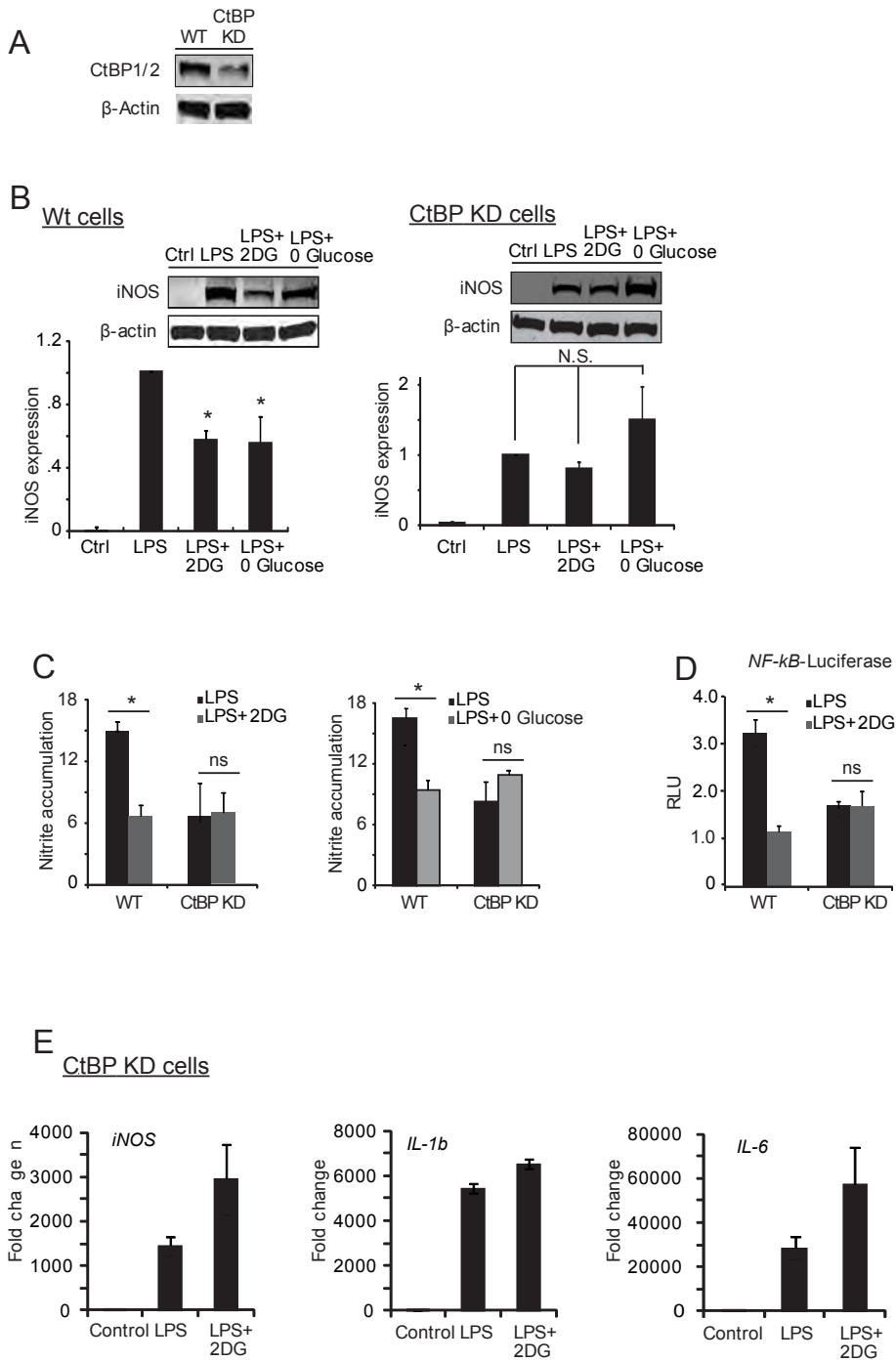


Figure 6

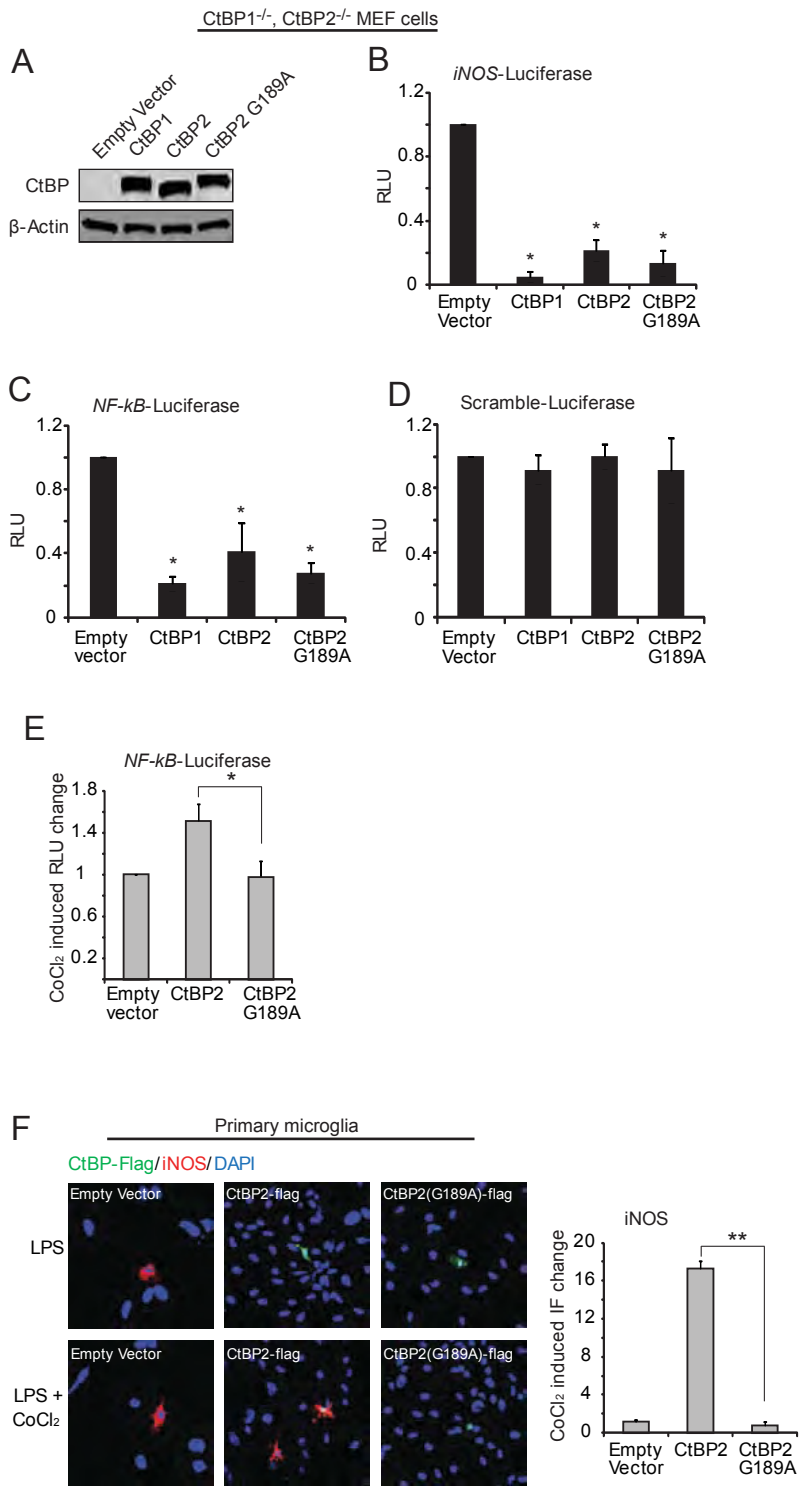
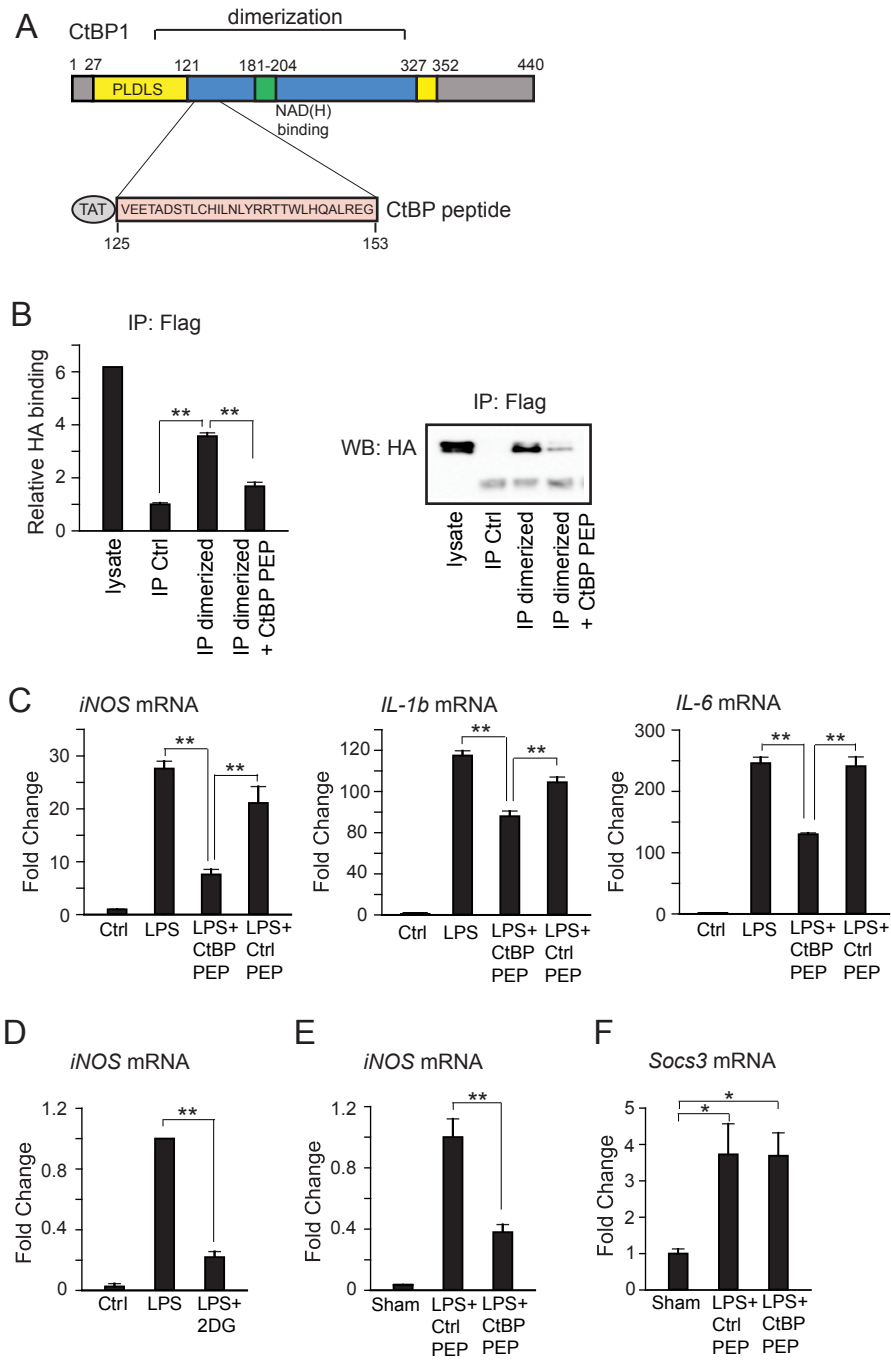


Figure 7



**Figure 8**

